Journal of Power Sources 246 (2014) 505–511

Contents lists available at ScienceDirect

Journal of Power Sources

journal homepage: www.elsevier.com/locate/jpowsour

Sub-micrometric $Li_{4-x}Na_xTi_5O_{12}$ ($0 \leq x \leq 0.2$) spinel as anode material exhibiting high rate capability

Ting-Feng Yi [a,c,d,*], Shuang-Yuan Yang [a], Xiao-Ya Li [a], Jin-Han Yao [b,**], Yan-Rong Zhu [a], Rong-Sun Zhu [a]

[a] School of Chemistry and Chemical Engineering, Anhui University of Technology, Maanshan, Anhui 243002, People's Republic of China
[b] State Key Laboratory Breeding Base of Green Chemistry-Synthesis Technology, College of Chemical Engineering and Material Science, Zhejiang University of Technology, Hangzhou, Zhejiang 310014, People's Republic of China
[c] Postdoctoral Research Station of Chemical Engineering & Technology, Harbin Institute of Technology, 150001 Harbin, People's Republic of China
[d] Chilwee Power Co. Ltd., Changxing, Zhejiang 313100, People's Republic of China

HIGHLIGHTS

- $Li_{4-x}Na_xTi_5O_{12}$ ($0 \leq x \leq 0.2$) anodes are first reported.
- Na doping improves the conductivity and reversibility of the $Li_4Ti_5O_{12}$.
- $Li_{4-x}Na_xTi_5O_{12}$ ($x = 0.1, 0.15$) anodes remarkably exhibit high rate performance.

ARTICLE INFO

Article history:
Received 19 May 2013
Received in revised form
31 July 2013
Accepted 2 August 2013
Available online 13 August 2013

Keywords:
Lithium-ion battery
Anode material
Rate capability
Lithium titanium oxide
Doping

ABSTRACT

The spinel $Li_4Ti_5O_{12}$ has been doped by Na for the purpose of improving its cycle performance as an anode. The lattice parameter of $Li_4Ti_5O_{12}$ increases due to the Na doping. SEM shows that all materials are well crystallized with a particle size in the range of 400–600 nm. The pristine $Li_4Ti_5O_{12}$ sample has a bigger particle size than that of Na-doped samples. Although the doping does not change the crystallographic structure of $Li_4Ti_5O_{12}$, they exhibit better cyclability at high charge–discharge rate compared with pristine $Li_4Ti_5O_{12}$. $Li_{3.85}Na_{0.15}Ti_5O_{12}$ gives the best cycling performance, only 11.1% loss of capacity after 80 cycles at 2 *C* charge–discharge rate. Na-doped $Li_4Ti_5O_{12}$ exhibits lower potential separation, indicating faster electron transfer kinetics and cycling reversibility. Electrochemical impedance spectroscopy demonstrates that the improved performance of the Na-doped $Li_4Ti_5O_{12}$ is due to a small decrease in the charge transfer resistance, indicating high electrochemical activity during cycling. The excellent cycling and safety performance of the Na-doped $Li_4Ti_5O_{12}$ electrodes are found to be due to the significantly increased ionic and electronic conductivity. Since fast charge–discharge performance is an important factor that needs to be considered in fabricating power batteries in industry, the Na-doped $Li_4Ti_5O_{12}$ materials moves closer to real and large scale applications.

1. Introduction

Among the currently available energy storage systems, the lithium-ion rechargeable battery has received intense attention from both the academic community and industry as the power source in hybrid electric vehicles (HEVs), plug-in hybrid electric vehicles (PHEVs), and full electric vehicles (EVs) due to the high energy density. But the intrinsically poor safety characteristics hindered the large-scale deployment of lithium-ion batteries. As we know, the current graphite anode material limits the application of LIBs as power batteries. The low charge–discharge plateau of graphite may lead to the deposition of metallic Li on the electrode at high current densities, causing serious safety problems [1]. The solid-electrolyte interphase (SEI) formed during the initial intercalation of lithium at about 0.8 V on the graphite surface tends to decompose at a temperature as low as 60 °C [2–4]. Thus, thermal stability of the SEI plays an important role in the safety of lithium-ion batteries. Fortunately, to address the safety limitations of Li-ion

* Corresponding author. School of Chemistry and Chemical Engineering, Anhui University of Technology, Maanshan, Anhui 243002, People's Republic of China. Tel.: +86 555 2311807; fax: +86 555 2311822.
** Corresponding author.
E-mail addresses: tfyihit@163.com (T.-F. Yi), jhyao@zjut.edu.cn (J.-H. Yao).

0378-7753/$ – see front matter © 2013 Elsevier B.V. All rights reserved.
http://dx.doi.org/10.1016/j.jpowsour.2013.08.005

cells, particularly those containing nickel-based cathodes ($LiNiO_2$), $Li_4Ti_5O_{12}$ (LTO) is an attractive anode material for power lithium-ion batteries [5,6]. It offers a convenient voltage-plateau at 1.5 V versus Li/Li^+ compatible with polymer electrolytes and high-voltage cathodes, thereby providing an electrode system with much better safety characteristics [7]. More importantly, $Li_4Ti_5O_{12}$ was formed at below 0.7 V in the first discharge process, but it is a SEI film free material when it was cycled above 1.0 V [8,9]. However, the disadvantage of LTO is its poor electronic conductivity that limits its full capacity at high charge–discharge rates. In order to overcome the significant drawbacks, two typical approaches have been developed to improve the rate capability of $Li_4Ti_5O_{12}$. One way is to enhance its electronic conductivity by doping with metal or non-metal ions (Mg^{2+} [10], Zn^{2+} [11], Al^{3+} [12], La^{3+} [13], Zr^{4+} [14], V^{5+} [15], Nb^{5+} [16], Mo^{6+} [17], F^- [18] and Br^- [19]) in Li, Ti or O sites or surface modification via coating conductive species including Ag [20], carbon [21], carbon nanotubes [22], polyacene (PAS) [23], TiN [24] and SnO_2 [25], etc. The other route is to synthesize nanostructured $Li_4Ti_5O_{12}$ materials [26]. However, Ceder et al. [27] reported that the particle size may not be the critical factor affecting the electrochemical performance of the electrode material. Also, decreasing the $Li_4Ti_5O_{12}$ particle size to the nano-scale results in an anode with very low powder tap density, and then significantly decreases the volumetric energy density of the cell [28]. Many methods have been proposed to prepare $Li_4Ti_5O_{12}$, such as solid-state reaction [15], sol–gel [29], microwave irradiation method [30], modified rheological phase reaction [31], cellulose-assisted combustion synthesis [32], molten-salt synthesis [33], and so on. However, it is difficult to commercial applications because of their complicated synthetic routes and high synthetic cost. From a commercial viewpoint, the solid-state synthesis of $Li_4Ti_5O_{12}$ powders exhibits a potential commercial application due to the simple synthesis route and low synthesis cost. It has been reported that Na doping can be considered as an effective way to improve the electrochemical performance of $LiFePO_4$ [34] and $Li_3V_2(PO_4)_3$ [35] positive-electrode material. To our knowledge, doping the spinel LTO with a low content of sodium has not been reported until now. Na-doped spinel LTO is expected, as Na-doped $LiFePO_4$, to have better rate ability and cycle performance. It is well known that the sodium is abundant and less expensive than the many transition metals and lithium metal, so Na substituted $Li_4Ti_5O_{12}$ spinel is expected to be an anode material with lower cost than other transition metals substituted $Li_4Ti_5O_{12}$. Hence, Na-doped spinel LTO compounds were prepared by a solid-state method using Na_2CO_3 as raw material. The electrochemical performances of Na-doped spinel LTO, including cycling stability and rate capability, were extensively evaluated in half cells.

2. Experimental

2.1. Material preparation

The Na-doped powder samples were prepared by a solid-state method. A mixture of TiO_2, Li_2CO_3 and Na_2CO_3 in proper amount was mixed by ball milling for 5 h in acetone slurry, followed by drying at 80 °C for 12 h. Then, the powders were calcined at 850 °C for 24 h in a flowing air atmosphere to obtain the samples.

2.2. Material characterization

Differential thermal analysis (DTA) and thermogravimetry (TG) measurements were performed in air from room temperature to 850 °C with a Henjiu Chare Tianping-1/2 thermal analysis system (Beijing, China) under a scanning rate of 5 °C min^{-1}. The X-ray diffractometry (XRD) measurements were performed on a Rigaku instrument with Cu Kα radiation. The Raman spectra were recorded at room temperature with a Renishaw inVia 1000 micro-Raman system using a 514.2 nm excitation line from an Ar+-ion laser (300 mW). Scanning electron microscopy (SEM) was performed to observe the particles morphology and analyze their composition. Cyclic voltammetry (CV) test was carried out on a CHI-852C electrochemical workstation with a voltage between 1 and 3 V at a scanning rate of 0.2 mV s^{-1}. Electrochemical impedance spectroscopy (EIS) is measured by a CHI 760D (Shanghai Chenhua, China) electrochemical working station over a frequency range from 0.01 Hz to 10 kHz at a potentiostatic signal amplitude of 5 mV. The prepared electrode materials were adopted as the work electrode; the counter electrode and reference electrode were Li foil. Galvanostatic charge/discharge cycles for batteries were recorded on multichannel Land Battery Test System (Wuhan Jinnuo, China) at different charge–discharge rates between 1 and 3 V (versus Li/Li^+).

2.3. Battery preparation

The working electrode was prepared by mixing a slurry of 80 wt % active material, 10 wt% acetylene black and 10 wt% polyvinylidene fluoride in *N*-methylpyrolline and then pasting it onto a Cu foil. After coating, the film was dried in a vacuum oven at 120 °C for 12 h and then cut into discs with a diameter of 14 mm. The coin cells were fabricated with the $Li_{4-x}Na_xTi_5O_{12}$, metallic lithium negative electrode, 1 M $LiPF_6$ in 1:1 diethyl carbonate/ethylene carbonate electrolyte, and Celgard polypropylene separator. All the batteries were conducted in an Ar-filled glove box (Etelux, China).

3. Results and discussion

Fig. 1 shows the TG-DTA curve of the well-proportioned mixed precursors (Li_2CO_3, TiO_2 and Na_2CO_3) after ball milled and dried in vacuum chamber. It can be found that there are two distinct steps of the weight loss in the TG curve. The first one is the interval between room temperature and 150 °C, and the preliminary weight loss is about 1%, mainly due to the evaporation of the absorbed water on the surface of the precursor mixture. In the second region 450–630 °C, the endothermic peak observed at 626 °C is accompanied by noticeable weight lose in the TG curve. It can be considered as a result of the decomposition of the inorganic constituents of the precursor followed by crystallization of spinel $Li_{3.85}Na_{0.15}Ti_5O_{12}$ phase. After 630 °C, the TG plot is stationary. It indicated that the decomposition has almost completed and all reactions have finished at the temperature of 630 °C. Therefore, it is necessary to calcine the precursor mixture above 630 °C to obtain the well-

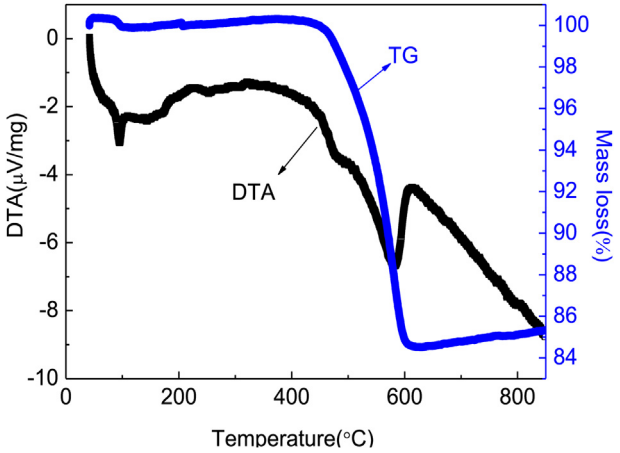

Fig. 1. TG-DTA curves of the mixture of $Li_{3.85}Na_{0.15}Ti_5O_{12}$ precursor powders.

crystallized $Li_{3.85}Na_{0.15}Ti_5O_{12}$. In this study, thermal conversion into $Li_{4-x}Na_xTi_5O_{12}$ with subsequent crystalline growth was prepared by heat treatment at 850 °C for 24 h.

The XRD patterns of as-synthesized $Li_{4-x}Na_xTi_5O_{12}$ ($0 \le x \le 0.2$) materials are shown in Fig. 2. All diffraction peaks observed for the prepared samples were assigned to expected reflections of spinel structure with *Fd*-3*m* space group. This means that the low dose doping of Na^+ does not alter the structure of materials. It can be observed that the patterns for $Li_{4-x}Na_xTi_5O_{12}$ ($x = 0, 0.05$) represent a single-phase cubic material without any impurity. However, there are few weak reflections corresponding to the impurity phase in the $Li_{4-x}Na_xTi_5O_{12}$ ($0.1 \le x \le 0.2$) samples, indicating that little Na ions do not enter the crystal lattice. The reason may be due to the great difference of ionic radius between Na^+ (1.02 Å) and Li^+ (0.76 Å) [36]. According to the enlarged peak of (1 1 1) planes of the samples, it can be concluded that the samples with the Na-doping undergo a slight shift toward lower degrees. This reveals that the lattice parameter increases due to the Na doping. The increased lattice parameter is ascribed to the larger Na^+ that occupied the sites of the smaller Li^+. The enlarged lattice constant is beneficial for fast lithium-ion transfer without lattice stability damaged [16].

Raman spectra of $Li_{4-x}Na_xTi_5O_{12}$ ($0 \le x \le 0.1$) powders are shown in Fig. 3. It can be found that there are five main Raman bands peaked at about 263, 342, 424, 671, and 745 cm^{-1} representing the features of the spinel structure ($A_{1g} + E_g + 3F_{2u}$) [37,38]. There are no obvious differences of Raman signals between $Li_4Ti_5O_{12}$ and $Li_{3.9}Na_{0.1}Ti_5O_{12}$ powders. However, it can be found

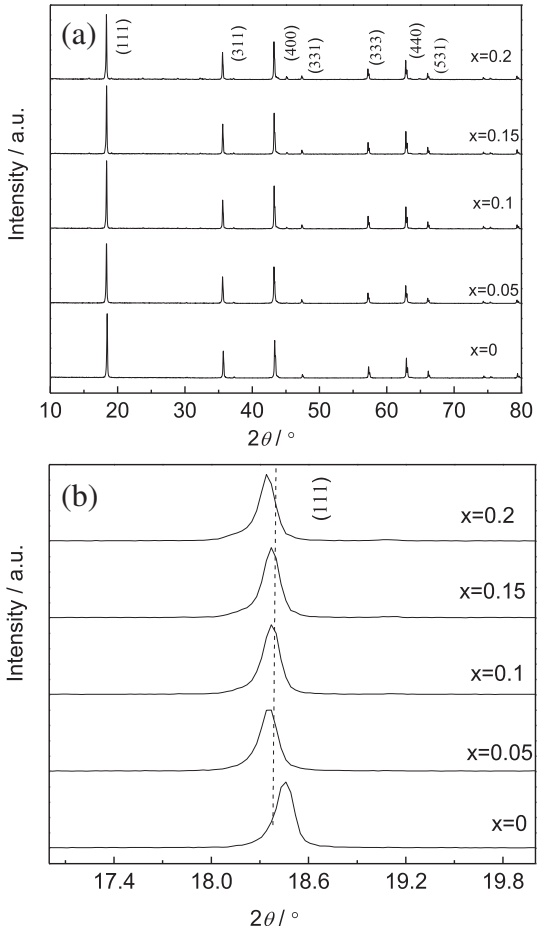

Fig. 2. (a) XRD patterns (b) enlarged (111) peaks of the $Li_{4-x}Na_xTi_5O_{12}$ ($x = 0, 0.05, 0.1, 0.15, 0.2$) materials.

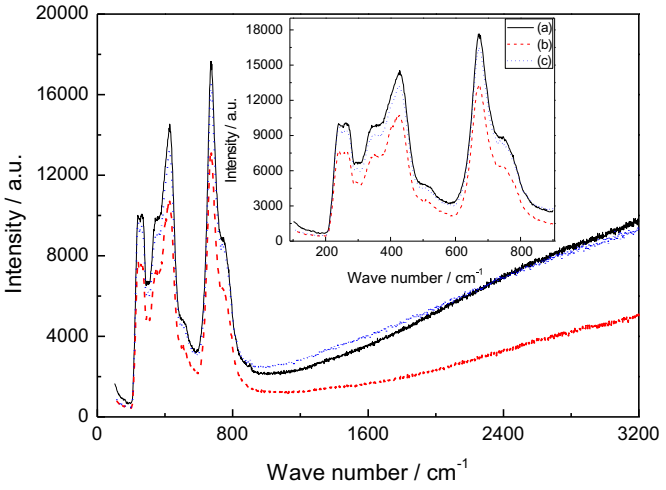

Fig. 3. Raman spectra of (a) $Li_4Ti_5O_{12}$, (b) $Li_{3.95}Na_{0.05}Ti_5O_{12}$ and (c) $Li_{3.9}Na_{0.1}Ti_5O_{12}$ powders.

that $Li_{3.95}Na_{0.05}Ti_5O_{12}$ shows a low Raman signals. The reason may be that there is a lower homogeneity in $Li_{3.95}Na_{0.05}Ti_5O_{12}$ because the low dose Na^+ ions doping ($x = 0.05$) may result in an increased confused degree of ion locations during long time high temperature sintering. In addition, it has been reported that the Raman signal intensity decreases as particle size increases [39]. This indicates that $Li_{3.95}Na_{0.05}Ti_5O_{12}$ may have a relative bigger particle size than that of other samples. This observation demonstrated the doping of Na^+ cannot change vibration characteristic of LTO, and this also indicates that Na doping cannot change the basic $Li_4Ti_5O_{12}$. The two higher frequency bands (674 and 744 cm^{-1}) are assigned to the vibrations of Ti–O bonds in TiO_6 octahedra. The middle frequency bands in the range of Raman shift 300–500 cm^{-1} can be assigned to the stretching vibrations of the Li–O bonds in LiO_4 and LiO_6 polyhedra, respectively [38]. No vibration bands were observed at about 1000–1600 cm^{-1}, which excludes the presence of trace impurities such as Na_2CO_3 and Li_2CO_3 in the final product [40,41].

Morphology of the as-prepared $Li_{4-x}Na_xTi_5O_{12}$ ($0 \le x \le 0.15$) in Fig. 4 shows that the materials are well crystallized with a particle size in the range of 400–600 nm. The pristine $Li_4Ti_5O_{12}$ sample has a bigger particle size than that of Na-doped samples. The small particle size of $Li_{4-x}Na_xTi_5O_{12}$ ($0.1 \le x \le 0.15$) results in sufficient contact between active materials and electrolyte and results in favorable diffusion and transmission of Li^+ in the electrode. This type of interconnected morphology of Na-doped $Li_4Ti_5O_{12}$ may help the transferring process of Li^+ ions and allow a better rate performance.

The initial charge–discharge curves of $Li_{4-x}Na_xTi_5O_{12}$ ($0 \le x \le 0.2$) at 0.1 C rates are shown in Fig. 5. The C rates were calculated based on 1 C = 175 mA g^{-1}. At the 0.1 C rate, the initial discharge specific capacities of Na-doped LTO are higher than the theoretical capacity of spinel $Li_4Ti_5O_{12}$ (175 mAh g^{-1}). The reason may be explained associated with the following structure analysis. The large difference in the ionic radius of Na^+ (1.02 Å), and Li^+ (0.76 Å) can lead to lattice distortion, thus introducing defects in $Li_4Ti_5O_{12}$. It has been reported that the defects in $Li_4Ti_5O_{12}$ [42] and amorphous MoO_2 [43] can serve as Li^+ storage sites for improved lithium capacity and rate performance. Hence, the increased initial capacity of Na-doped $Li_4Ti_5O_{12}$ might also originate from the lattice distortion resulted from the substitution of Na^+ for Li^+. In addition, from the literature [44] it can be concluded that the $Li_4Ti_5O_{12}$ with small particle size can provide much larger initial capacity than that with large particle size. Hence, we speculate that this phenomenon may be related with the Na doing, micron-sized particles and so

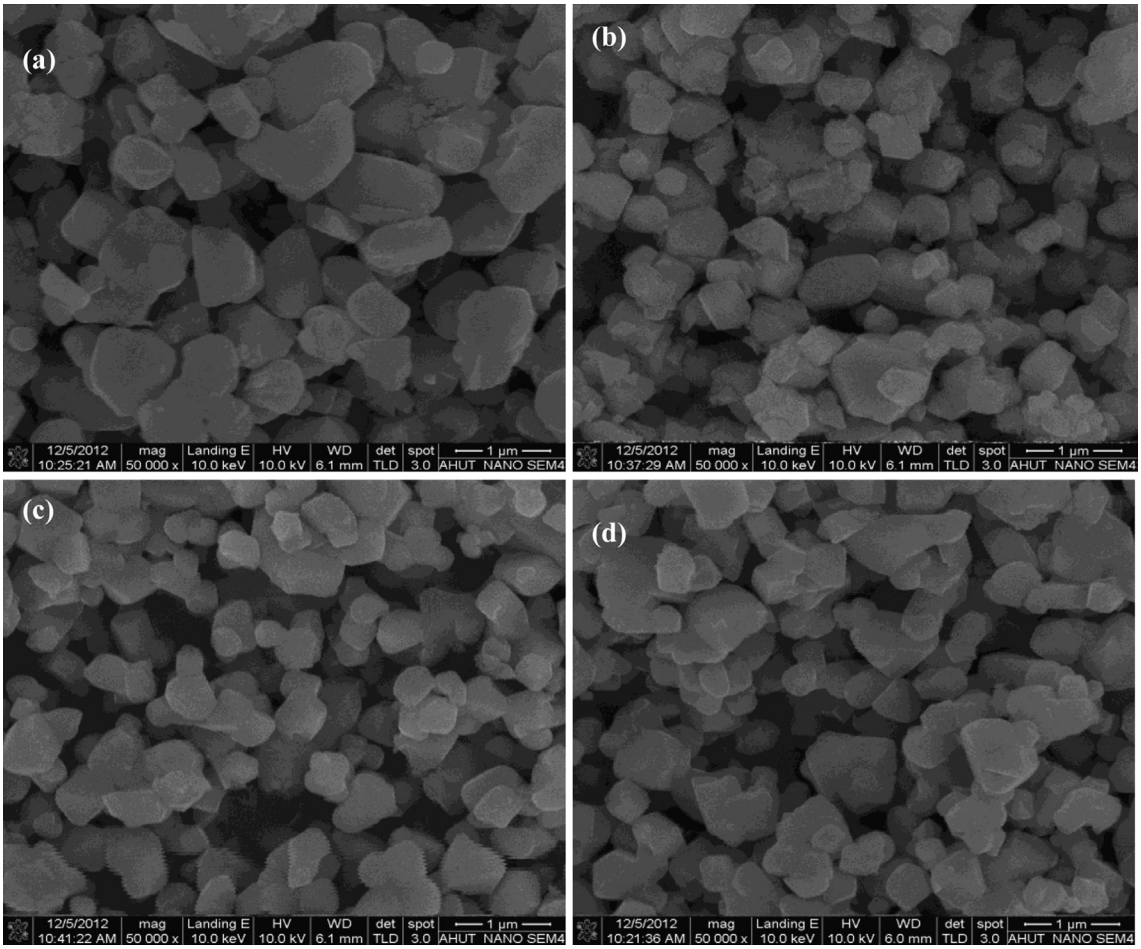

Fig. 4. SEM images of the as-prepared $Li_{4-x}Na_xTi_5O_{12}$ (a) $x = 0$, (b) $x = 0.05$, (c) $x = 0.1$, (d) $x = 0.15$.

small charge–discharge rates. The mechanism of formation needs further investigation, but it is assumed that the Na doing plays a decisive role in formation of the high discharge capacity.

Although the incorporation of Na^+ is expected to increase the conductivity of the samples, the larger ion radius of the Na^+ ions than that of the Li^+ ions may hinder the ion insertion. When the content of Na^+ is too low or too high, hindering effects may play a relatively leading role. Hence, it can be concluded that Na-doping with low ratio or high ratio cannot obviously improve the lithium ion diffusivity property of $Li_4Ti_5O_{12}$ (see Table 2). It has been reported that the insertion/extraction of lithium ions is rather sufficient even in bulk materials during the low charge–discharge current density [45,46]. However, $Li_{3.95}Na_{0.05}Ti_5O_{12}$ material shows a low plateau voltage at about 1.43 V shown in Fig. 5, suggesting increased polarization for the $Li_{3.95}Na_{0.05}Ti_5O_{12}$ electrode. As we know, the electrode material synthesized by solid-state method has a lower homogeneity than that prepared by soft chemical method [47]. Hence, we speculate that low dose Na^+ ions doping ($x = 0.05$) may result in an increased confused degree of ion locations during long time high temperature sintering. As the analysis of the Raman spectra, the increased confused degree may cause distortion of the internal crystal structure of $Li_4Ti_5O_{12}$, and even lead to the destruction of its crystal structure, so that $Li_{3.95}Na_{0.05}Ti_5O_{12}$ shows a low plateau voltage. In addition, from the Raman spectra results

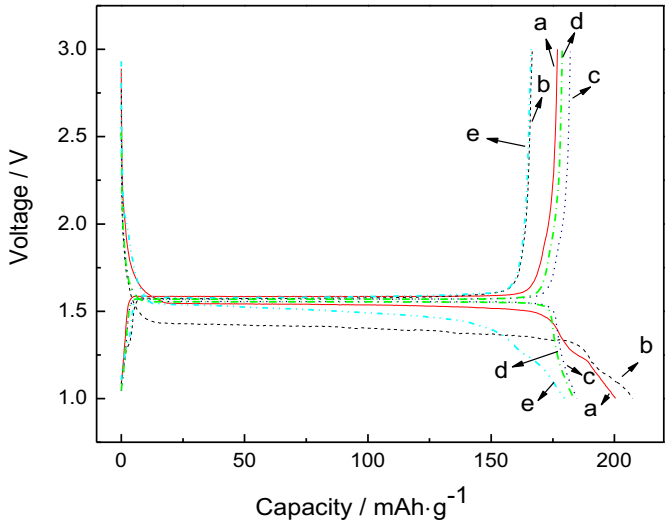

Fig. 5. Initial charge–discharge curves of $Li_{4-x}Na_xTi_5O_{12}$ at 0.1 C .(a) $x = 0$, (b) $x = 0.05$, (c) $x = 0.1$, (d) $x = 0.15$, (e) $x = 0.2$.

Table 1
Values of the CV peaks for $Li_{4-x}Na_xTi_5O_{12}$ ($x = 0$, 0.05, 0.1, 0.15, 0.2).

Samples	φ_{pa}(V)	φ_{pc}(V)	$\Delta\varphi_p$(mV)
$Li_4Ti_5O_{12}$	1.719	1.493	226
$Li_{3.95}Na_{0.05}Ti_5O_{12}$	1.683	1.511	172
$Li_{3.9}Na_{0.1}Ti_5O_{12}$	1.669	1.501	158
$Li_{3.85}Na_{0.15}Ti_5O_{12}$	1.700	1.500	200
$Li_{3.8}Na_{0.2}Ti_5O_{12}$	1.710	1.508	202

Table 2
Fitted results of $Li_{4-x}Na_xTi_5O_{12}$ ($0 \le x \le 0.2$) obtained by EIS.

Samples	$Li_4Ti_5O_{12}$	$Li_{3.95}Na_{0.05}Ti_5O_{12}$	$Li_{3.9}Na_{0.1}Ti_5O_{12}$	$Li_{3.85}Na_{0.15}Ti_5O_{12}$	$Li_{3.8}Na_{0.2}Ti_5O_{12}$
R_{ct}/Ω	555.4	172.1	150.8	229.7	391.3
$D_{Li}/cm^2\ s^{-1}$	3.43×10^{-17}	8.50×10^{-17}	2.00×10^{-15}	2.39×10^{-16}	8.13×10^{-17}
$\sigma/\Omega\ s^{-0.5}$	1491.5	948.0	195.5	565.8	969.1

mentioned above, $Li_{3.95}Na_{0.05}Ti_5O_{12}$ may have a relative bigger particle size than that of other samples, and then resulting in insufficient contact between active materials and electrolyte. We speculate that this may result in unfavorable diffusion and transmission of Li^+ in the electrode, and then lead a low plateau voltage of $Li_{3.95}Na_{0.05}Ti_5O_{12}$ during the first cycle.

The discharge capacity decreased to 130–140 mAh g^{-1} at charge–discharged at 0.5 C due to the difficulty in lithium migration between 8a and 16c sites in bulk materials (see Fig. 7). Fig. 6 shows the dQ/dV versus voltage plots for the $Li_{4-x}Na_xTi_5O_{12}$ ($0 \le x \le 0.2$) anode material between 1 and 3 V from Fig. 5. From Fig. 6, it is observed that the electrochemical insertion of lithium atoms into $Li_4Ti_5O_{12}$ is a two-phase process that forms a solid solution between $Li_4Ti_5O_{12}$ and $Li_7Ti_5O_{12}$, and that presents as a long voltage-plateau at 1.55 V vs. Li/Li^+. This indicates that the Na doping does not change the spinel structure and electrochemical reaction mechanism of $Li_4Ti_5O_{12}$.

Fig. 7 shows the cycle life performance and rate capabilities of the $Li_{4-x}Na_xTi_5O_{12}$ ($0 \le x \le 0.2$) at different C rates between 1 and 3 V in coin-type half cells. The charge and discharge rate is the same. It can be found that $Li_{4-x}Na_xTi_5O_{12}$ ($0.05 \le x \le 0.15$) anodes have higher discharge capacities than that of pristine $Li_4Ti_5O_{12}$ at each cycle. After 80 cycles, the discharge capacities of $Li_{4-x}Na_xTi_5O_{12}$ ($x = 0, 0.05, 0.1, 0.15, 0.2$) charge–discharged at 2 C rate were measured as 109.8, 134.9, 139.1, 139.4 and 111.3 mAh g^{-1}, respectively. The capacity of the $Li_{4-x}Na_xTi_5O_{12}$ ($x = 0.1, 0.15$) in the 80th cycle is about 1.27 times that of the pristine $Li_4Ti_5O_{12}$ particles. If the capacity obtained at 0.5 C is used as a standard, the capacity retention at the 2 C rate is 79.8%, 86.5%, 89.9%, 86.0% and 83.1% for $Li_{4-x}Na_xTi_5O_{12}$ ($x = 0, 0.05, 0.1, 0.15, 0.2$) anodes, respectively. That is, the Na-doped $Li_4Ti_5O_{12}$ exhibits excellent capacity and superior cycleability at high-rate charge/discharge, in comparison with pristine $Li_4Ti_5O_{12}$ particles. These test results also indicate that the Na-doped $Li_4Ti_5O_{12}$ is sufficiently stable for fast charge–discharge cycling. It is obvious that the excellent rate capability of Na-doped $Li_4Ti_5O_{12}$ originates from the submicron-size effect on one hand, but most importantly from the significantly increased ionic and electronic conductivity.

Fig. 8 shows the cyclic voltammetry (CV) of the coin cells containing $Li_{4-x}Na_xTi_5O_{12}$ ($x = 0, 0.05, 0.1, 0.15, 0.2$) as anode material. All measurements were taken at room temperature at a scan rate of 0.2 mV s^{-1} and in voltage range of 1–3 V (vs. Li/Li^+). The CV peaks were narrow and sharper, which corresponds to the oxidation process accompanied by delithiation of lithium ions from the lattices. The CVs of all samples exhibited a pair of redox peaks at about 1.5 and 1.7 V, which is characteristic for the lithium ion intercalation–deintercalation reaction between $Li_4Ti_5O_{12}$ and $Li_7Ti_5O_{12}$ phase. The CV peaks values of the various samples at scan rates of 0.2 mV s^{-1} are listed in Table 1. The potential separations between the anodic/cathodic peaks for the Na-doped $Li_4Ti_5O_{12}$ samples are lower than those of $Li_4Ti_5O_{12}$, indicating that Na doping is beneficial to the reversible intercalation and deintercalation of Li^+, and then enhances the reversibility of the $Li_4Ti_5O_{12}$ [17,48]. With the increase of Na doping concentration, the peak current reduced progressively, implying a drop in the electrode kinetics. The reason may be that the confusion degree of ion location increases due to the Na doping, and then results in a blocking effect for the lithium charge transfer from the electrolyte to the electrode. In addition, the potential separation can be determined by the potential polarization of the active material during charge and discharge process. Hence, the low potential separation demonstrates that the lithium insertion into the Na-doped $Li_4Ti_5O_{12}$ composite behaves more likely as a Nernst system [49]. Moreover, $Li_{3.9}Na_{0.1}Ti_5O_{12}$ exhibits the smallest potential separations among all samples, indicating faster electron transfer kinetics and cycling reversibility. This can be confirmed that $Li_{3.9}Na_{0.1}Ti_5O_{12}$ has the best electrochemical performance among the others.

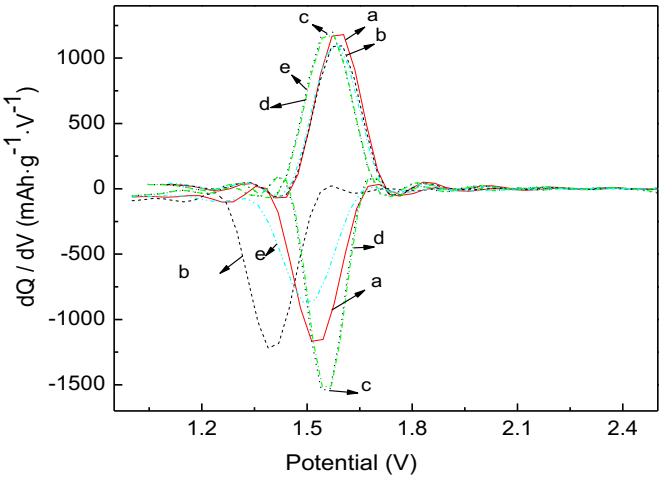

Fig. 6. Differential capacity vs voltage plots of $Li_{4-x}Na_xTi_5O_{12}$ from Fig. 5 (a) $x = 0$, (b) $x = 0.05$, (c) $x = 0.1$, (d) $x = 0.15$, (e) $x = 0.2$.

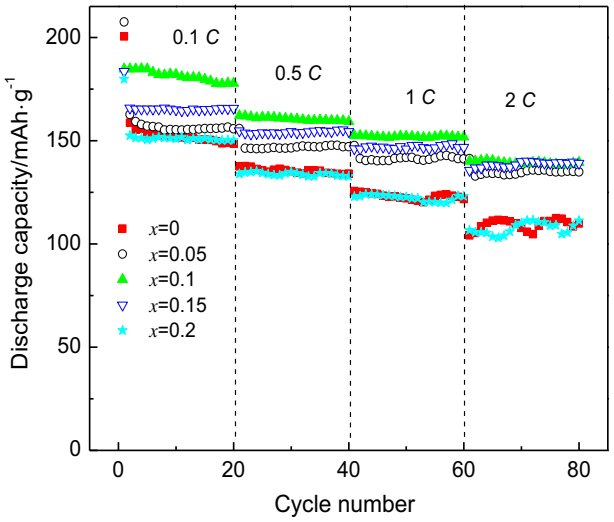

Fig. 7. Cycling performances and rate capabilities of $Li_{4-x}Na_xTi_5O_{12}$ ($x = 0, 0.05, 0.1, 0.15, 0.2$) at different charge–discharge rates in coin-type half cells (the charge and discharge rate were the same).

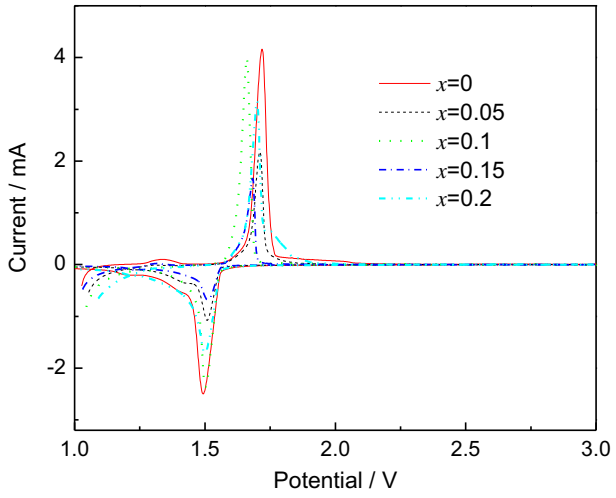

Fig. 8. Cyclic voltammetry (CV) of the $Li_{4-x}Na_xTi_5O_{12}$ (x = 0, 0.05, 0.1, 0.15, 0.2) samples.

An analysis of the EIS can differentiate the contribution of Li ion migration through the surface film, charge transfer through the electrode/electrolyte interface and the solid-state diffusion of Li ions in the cathode material [50]. Fig. 9 shows the Nyquist plots of the fresh $Li_{4-x}Na_xTi_5O_{12}$ ($x = 0, 0.05, 0.1, 0.15, 0.2$)/Li cells measured at room temperature. The enlarged Nyquist plots of $Li_{4-x}Na_xTi_5O_{12}$ ($0 \le x \le 0.2$) are as shown in Fig. 9 as an insert. The high-frequency semicircle always corresponds to the charge transfer process (R_{ct}), and the fitted R_{ct} data are listed in Table 2. It was found the overall charge transfer resistance of the Na-doped electrodes increased gradually with the increase of Na concentration, but it was much smaller than that of the pristine $Li_4Ti_5O_{12}$. $Li_{3.9}Na_{0.1}Ti_5O_{12}$ exhibits the smallest charge transfer resistance among all samples, suggesting that $Li_{3.9}Na_{0.1}Ti_5O_{12}$ may have the highest electrochemical activity during cycling. The straight line with a slope of approximately 45° in low frequency region is attributed to the diffusion of the lithium ions into the bulk of the electrode material or so-called Warburg diffusion. The lithium ion diffusion coefficient (D_{Li}) is calculated according to the following equation [51–53]:

$$D_{Li} = \frac{(RT)^2}{2(An^2F^2C_{Li}\sigma)^2} \quad (1)$$

where the meanings of n is the number of electrons transferred in the half-reaction for the redox couple, which is equal to 1 [53], A the surface area of the electrode (1.54 cm^2), R the gas constant (8.314 J mol^{-1} K^{-1}), T the absolute temperature (298 K), F the Faraday constant (96500 C mol^{-1}), C_{Li} the concentration of lithium ion in solid (4.37 × 10^{-3} mol cm^{-3}) [53], and σ is the Warburg factor which has relationship with Z_{re}:

$$Z_{re} = R_{ct} + R_s + \sigma\omega^{-\frac{1}{2}} \quad (2)$$

Fig. 10 shows the relationship between Z_{re} and square root of frequency ($\omega^{-1/2}$) in the low frequency region. The diffusion coefficient of lithium ion can be calculated based on Eqs. (1) and (2), and the calculated result is given in Table 2. It indicates the Na doping has a positive effect on the electrode performance, the increase of electronic conductivity and lithium ion diffusivity. $Li_{3.9}Na_{0.1}Ti_5O_{12}$ exhibits the largest lithium diffusion coefficient among all samples, suggesting that $Li_{3.9}Na_{0.1}Ti_5O_{12}$ may have the highest electrochemical activity during cycling.

Although, excellent cyclability with high rate discharge contributed to the commercial success of lithium-ion rechargeable batteries, future applications, like HEV, PHEV require a fast charge capability. Fast charge can induce severe underpotential, resulting in hazardous Li plating and the subsequent deterioration of cell performance [45]. Hence, it is important to focus on the high rate charge–discharge performance of as-prepared $Li_4Ti_5O_{12}$ material. To provide more information about the difference in electrochemical performances of the Na-doped $Li_4Ti_5O_{12}$, high rate charge–discharge measurements were carried out on $Li_{4-x}Na_xTi_5O_{12}$ ($0 \le x \le 0.15$) anode at 5 C charge–discharge rate as presented in Fig. 11. As shown in this figure, one can see the $Li_{4-x}Na_xTi_5O_{12}$ ($x = 0.1, 0.15$)/Li cells exhibits discharge capacities of ca. 133 and 135 mAh g^{-1}, respectively, after 200 cycles at the high charge–discharge rate of 5 C. After 200 charge–discharge cycles, the $Li_{4-x}Na_xTi_5O_{12}$ ($x = 0.1, 0.15$) electrodes exhibit excellent cycling performance with capacity retention ratio of near 100%. However, the pristine $Li_4Ti_5O_{12}$/Li cells only exhibits discharge capacity of ca. 93 mAh g^{-1} after 200 cycles. The superior cycling performance at

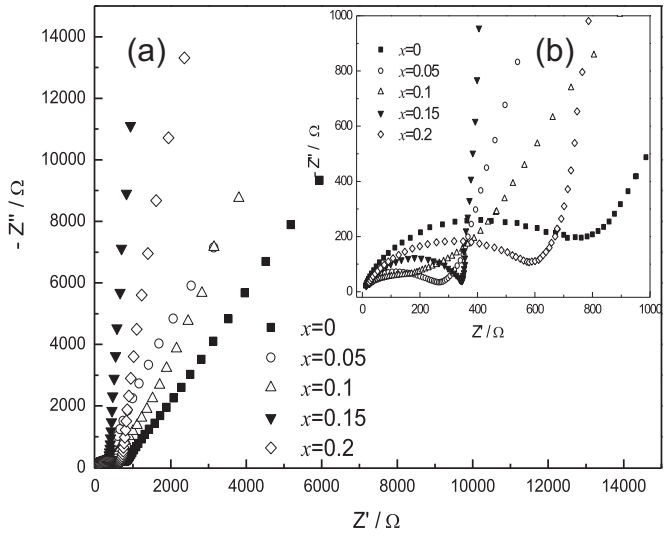

Fig. 9. Nyquist plots of $Li_4Ti_{5-x}Na_xO_{12}$ ($x = 0, 0.05, 0.1, 0.15, 0.2$) materials (a) $x = 0$, (b) $x = 0.05$, (c) $x = 0.1$, (d) $x = 0.15$, (e) $x = 0.2$.

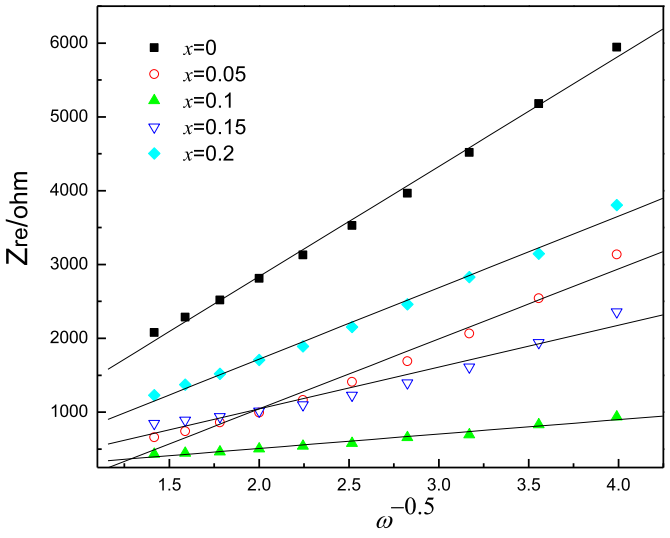

Fig. 10. Graph of Z_{re} plotted against $\omega^{-1/2}$ at low frequency region for $Li_{4-x}Na_xTi_5O_{12}$ ($x = 0, 0.05, 0.1, 0.15, 0.2$) electrodes.

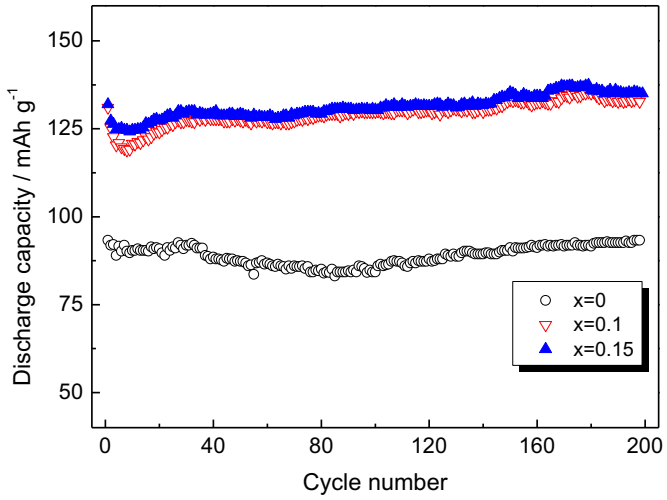

Fig. 11. High charge–discharge rate cycling performance of $Li_{4-x}Na_xTi_5O_{12}$ (x = 0, 0.1, 0.15)/Li cells at 5 *C* charge–discharge rate in the voltage range between 1 and 3 V.

high charge–discharged rates shows that Na-doped $Li_4Ti_5O_{12}$ materials have very high structural stability and outstanding reversibility even after 200 cycles at high charge–discharge rate, and further proves that appropriate amount doping cannot change the basic $Li_4Ti_5O_{12}$ structure. The improved electrode performance of Na-doped $Li_4Ti_5O_{12}$ is clearly related to the improved electronic conductivity and lithium ion diffusivity.

4. Conclusions

Single phase $Li_{4-x}Na_xTi_5O_{12}$ (x = 0, 0.05, 0.1, 0.15, 0.2) spinels have been synthesized by an easy solid-state method. The morphological characterization shows that all samples have homogeneous sub-micrometric particle size (400–600 nm) and it is very well-crystallized. $Li_{4-x}Na_xTi_5O_{12}$ (x = 0.1, 0.15) materials exhibit the highest rate capability among the $Li_4Ti_5O_{12}$-type anodes. The capacity retentions of $Li_{3.9}Na_{0.1}Ti_5O_{12}$ spinel is over 89% after 80 cycles at 2C charge–discharge rate. $Li_{4-x}Na_xTi_5O_{12}$ (x = 0.1, 0.15)/Li cells exhibits discharge capacities of ca. 133 and 135 mAh g^{-1}, respectively, after 200 cycles at the high charge–discharge rate of 5 *C*. The improved electrode performance of Na-doped $Li_4Ti_5O_{12}$ is clearly related to the improved electronic conductivity and lithium ion diffusivity. These outstanding electrochemical performances demonstrate the $Li_{4-x}Na_xTi_5O_{12}$ (x = 0.1, 0.15) as a very promising anode for practical high-power lithium-ion battery needed for hybrid and electric vehicles.

Acknowledgments

This work was financially supported by the National Natural Science Foundation of China (nos. 51274002 and 50902001), the China Postdoctoral Science Foundation (no. 2012M520749), the Zhejiang Postdoctoral Preferential Foundation (No. Bsh1201013), and the Program for Innovative Research Team in Anhui University of Technology (no. TD201202).

References

[1] S.S. Zhang, J. Power Sources 161 (2006) 1385–1391.
[2] M. Holzapfel, F. Alloin, R. Yazami, Electrochim. Acta 49 (2004) 581–589.
[3] Z.H. Chen, Y. Qin, Y. Ren, W.Q. Lu, C. Orendorff, E.P. Roth, K. Amine, Energy Environ. Sci. 4 (2011) 4023–4030.
[4] J. Shu, Electrochem. Solid-State Lett. 11 (2008) A238–A240.
[5] T. Ohzuku, A. Ueda, N. Yamamoto, J. Electrochem. Soc. 142 (1995) 1431–1435.
[6] E. Ferg, R.J. Gummow, A. de Kock, M. Thackeray, J. Electrochem. Soc. 141 (1994) L147–L150.
[7] T.-F. Yi, L.-J. Jiang, J. Shu, C.-B. Yue, R.-S. Zhu, H.-B. Qiao, J. Phys. Chem. Solids 71 (2010) 1236–1242.
[8] T.-F. Yi, J. Shu, Y.-R. Zhu, X.-D. Zhu, C.-B. Yue, A.-N. Zhou, R.-S. Zhu, Electrochim. Acta 54 (2009) 7464–7470.
[9] G.X. Wang, D.H. Bradhurst, S.X. Dou, H.K. Liu, J. Power Sources 83 (1999) 156–161.
[10] C.H. Chen, J.T. Vaughey, A.N. Jansen, D.W. Dees, A.J. Kahaian, T. Goacher, M.M. Thackeray, J. Electrochem. Soc. 148 (2001) A102–A104.
[11] B. Zhang, H. Du, B. Li, F. Kang, Electrochem. Solid-State Lett. 13 (2010) A36–A38.
[12] H. Zhao, Y. Li, Z. Zhu, J. Lin, Z. Tian, R. Wang, Electrochim. Acta 53 (2008) 7079–7083.
[13] T.-F. Yi, Y. Xie, Q. Wu, H. Liu, L. Jiang, M. Ye, R. Zhu, J. Power Sources 214 (2012) 220–226.
[14] X. Li, M. Qu, Z. Yu, J. Alloys Compd. 487 (2009) L12–L17.
[15] P. Kubiak, A. Garcia, M. Womes, L. Aldon, J. Olivier-Fourcade, P.-E. Lippens, J.-C. Jumas, J. Power Sources 119–121 (2003) 626–630.
[16] B. Tian, H. Xiang, L. Zhang, Z. Li, H. Wang, J. Solid State Electrochem. 16 (2012) 205–211.
[17] T.-F. Yi, Y. Xie, L.-J. Jiang, J. Shu, C.-B. Yue, A.-N. Zhou, M.-F. Ye, RSC Adv. 2 (2012) 3541–3547.
[18] S. Huang, Z. Wen, Z. Gu, X. Zhu, Electrochim. Acta 50 (2005) 4057–4062.
[19] Y. Qi, Y. Huang, Di. Jia, S.-J. Bao, Z.P. Guo, Electrochim. Acta 54 (2009) 4772–4776.
[20] S. Huang, Z. Wen, J. Zhang, X. Yang, Electrochim. Acta 52 (2007) 3704–3708.
[21] J. Gao, J. Ying, C. Jiang, C. Wan, J. Power Sources 166 (2007) 255–259.
[22] J. Huang, Z. Jiang, Electrochim. Acta 53 (2008) 7756–7759.
[23] H. Yu, X. Zhang, A.F. Jalbout, X. Yan, X. Pan, H.g. Xie, R. Wang, Electrochim. Acta 53 (2008) 4200–4204.
[24] K.-S. Park, A. Benayad, D.-J. Kang, S.-G. Doo, J. Am. Chem. Soc. 130 (2008) 14930–14931.
[25] Y.-Y. Wang, Y.-J. Hao, Q.-Y. Lai, J.-Z. Lu, Y.-D. Chen, X.-Y. Ji, Ionics 14 (2008) 85–88.
[26] H.W. Lu, W. Zeng, Y.S. Li, Z.W. Fu, J. Power Sources 164 (2007) 874.
[27] X. Ma, B. Kang, G. Ceder, J. Electrochem. Soc. 157 (2010) A925–A931.
[28] H.-G. Jung, S.-T. Myung, C.S. Yoon, S.-B. Son, K.H. Oh, K. Amine, B. Scrosati, Y.-K. Sun, Energy Environ. Sci. 4 (2011) 1345–1351.
[29] Y.-J. Hao, Q.-Y. Lai, J.-Z. Lu, H.-L. Wang, Y.-D. Chen, X.-Y. Ji, J. Power Sources 158 (2006) 1358–1364.
[30] J. Li, Y.-L. Jin, X.-G. Zhang, H. Yang, Solid State Ionics 178 (2007) 1590–1594.
[31] S.Y. Yin, L. Song, X.Y. Wang, M.F. Zhang, K.L. Zhang, Y.X. Zhang, Electrochim. Acta 54 (2009) 5629–5633.
[32] T. Yuan, K. Wang, R. Cai, R. Ran, Z. Shao, J. Alloys Compd. 477 (2009) 665–672.
[33] Y. Bai, F. Wang, F. Wu, C. Wu, L.-y Bao, Electrochim. Acta 54 (2008) 322–327.
[34] X. Yin, K. Huang, S. Liu, H. Wang, H. Wang, J. Power Sources 195 (2010) 4308–4312.
[35] Q. Kuang, Y. Zhao, Z. Liang, J. Power Sources 196 (2011) 10169–10175.
[36] R.D. Shannon, Acta Crystallogr. A32 (1976) 751–767.
[37] L. Aldon, P. Kubiak, M. Womes, J.C. Jumas, J. Olivier-Fourcade, J.L. Tirado, J.I. Corredor, C. Pérez Vicente, Chem. Mater. 16 (2004) 5721–5725.
[38] R. Baddour-Hadjean, J.-P. Pereira-Ramos, Chem. Rev. 110 (2010) 1278–1319.
[39] M.V. Pellow-Jarman, P.J. Hendra, R.J. Lehnert, Vib. Spectrosc. 12 (1996) 257–261.
[40] J.F. Widmann, C.L. Aardahl, E.J. Davis, TrAC Trends Anal. Chem. 17 (1998) 339–345.
[41] P. Pasierb, S. Komornicki, M. Rokita, M. Rękas, J. Mol. Struct. 596 (2001) 151–156.
[42] X. Chen, X. Guan, L. Li, G. Li, J. Power Sources 210 (2012) 297–302.
[43] J.H. Ku, J.H. Ryu, S.H. Kim, O.H. Han, S.M. Oh, Adv. Func. Mater. 22 (2012) 3658–3664.
[44] W.J.H. Borghols, M. Wagemaker, U. Lafont, E.M. Kelder, F.M. Mulder, J. Am. Chem. Soc. 131 (2009) 17786–17792.
[45] G.G. Amatucci, F. Badway, A.D. Pasquier, T. Zheng, J. Electrochem. Soc. 148 (2001) A930–A939.
[46] S. Ji, J. Zhang, W. Wang, Y. Huang, Z. Feng, Z. Zhang, Z. Tang, Mater. Chem. Phys. 123 (2010) 510–515.
[47] C. Zhang, Y. Zhang, J. Wang, D. Wang, D. He, Y. Xia, J. Power Sources 236 (2013) 118–125.
[48] B. Tian, H. Xiang, L. Zhang, Z. Li, H. Wang, Electrochim. Acta 55 (2010) 5453–5458.
[49] L. Xiao, Y. Zhao, Y. Yang, Y. Cao, X. Ai, H. Yang, Electrochim. Acta 54 (2008) 545–550.
[50] K.M. Shaju, R.G.V. Subba, B.V.R. Chowdari, J. Mater. Chem. 13 (2003) 106.
[51] A.Y. Shenouda, H.K. Liu, J. Power Sources 185 (2008) 1386–1391.
[52] Q. Cao, H.P. Zhang, G.J. Wang, Q. Xia, Y.P. Wu, H.Q. Wu, Electrochem. Commun. 9 (2007) 1228–1232.
[53] S.-L. Chou, J.-Z. Wang, H.-K. Liu, S.-X. Dou, J. Phys. Chem. C 115 (2011) 16220–16227.